Proc. Natl. Sci Counc. ROC(A)
Vol. 19, No. 5, 1995. pp. 463-479

A Numerical Study of Pollutant Distributions with Presumptive Sources during Frontal Formation

CHING-YUANG HUANG

Department of Atmospheric Sciences
National Central University
Chung-Li, Taiwan, R.O.C.

(Received August 12, 1994; Accepted March 17, 1995)

ABSTRACT

Advection-diffusion processes of presumptive instantaneous pollutant sources are investigated for coastal environmental conditions where frontogenesis appears in response to differential heating. The investigation relies on a mesoscale planetary-boundary-layer (PBL) numerical model which includes the modified E-ε turbulence closure and cloud microphysics for resolving turbulence activities within the PBL and clouds. Model results from control numerical experiments show that the cloud and pollutant distributions during the frontal formation and flow deformation are sensitive to variations in ambient wind speed, vertical moisture profile and wind shear, and the height and location of the neighboring terrain barrier. The effects due to these factors are discussed in detail in this study. It is found that the advection-diffusion processes of the pollutants are rather complicated in coastal varying wind and stability conditions. The relative importance of turbulent diffusion and mean transport is also discussed with relevance to the source height and emission time.

Key Words: advection-diffusion, PBL, frontal formation

I. Introduction

Air pollution has been recognized as a big problem for people who live in highly polluted areas. Coastal releases of air pollutants, for example from mobile vehicles and huge power plants, in particular produce severe situations at which variations in dispersion could significantly influence people due to the characteristic features of coastal flow evolution. An obvious example is dispersion under sea breeze circulations which are known to be sometimes associated with a strong returning flow which brings pollutants back to inland regions (Segal *et al.*, 1982; Pielke *et al.*, 1983). As the mesoscale dynamics are involved in the diffusion processes of coastal pollutants, the gross behaviors of the sum of each individual source release cannot be simply described by conventional air dispersion models. Release of individual small sources may obey statistical prediction of Gaussian-type formulas provided there are favorable quasi-steady meteorological conditions (Pasquill, 1974; Hanna, 1982). The air pollution due to such small area sources or continuous point sources generally has only a local impact because of the tiny spatial scale. However, such in-site diffusion, once combined into a format of wider area pollution such as metropolitan pollution, could be significantly redistributed by mesoscale circulation, and the geometric patterns should be regionally important. Understanding the various processes of regional air pollutant transport is, thus, important and requires knowledge of the effects of mesoscale complex flow on pollutant distribution.

A number of numerical modeling studies have been devoted to the advection-diffusion processes of air pollutants in complex atmospheric environments (Shir and Shieh, 1974; Bornstein and Runca, 1977; MacCracken *et al.*, 1978; Anthes and Warner, 1978; Segal *et al.*, 1982; Pielke *et al.*, 1983; Arritt *et al.*, 1988). In the determination of SO_2 distribution in the St. Louis metropolitan area, Shir and Shieh (1974) obtained good estimation by solving the concentration equation with interpolated observation input. On the other hand, mesoscale hydrostatic models have been developed to investigate air pollution under transient meteorological conditions (Anthes and Warner, 1978). Segal *et al.* (1982) used a mesoscale model to directly simulate the redistribution of air pollutants in the vicinity of the Chesapeake Bay, and the simulated mesoscale fields were further interpolated to provide detailed meteorological conditions for use in a finer-scale dispersion model (Pielke *et al.*, 1983). The potential impact of second-time pollution due to recirculation in the later stage of sea breeze development has been well-exhibited by numerical studies. With the help of a

mesoscale model, pollution in the range of 2-20 km (i.e., the meso-γ scale as conventionally defined) can be more reasonably described since validity of empirical and statistical dispersion models is questionable in application to this scale. Pielke *et al.* (1983) have demonstrated the advantages of using a mesoscale numerical model for evaluations of pollutant transport and diffusion over coastal complex terrain.

There have been few numerical studies related to coastal pollution during frontal formation and flow deformation. Over the coastal baroclinic zone that originates from air-water temperature differences, fronts can be generated through differential heating (Huang and Raman, 1992). As the ambient flow is onshore, a quasi-stationary front may form over the boundary of thermal variations as indicated by a climatological study for the New England coastal frontogenesis (Bosart, 1975). Three-dimensional numerical simulations (Huang and Raman, 1992) have confirmed this possible mechanism, where coastal deformational flow occurs ultimately in response to the effects of the underlying baroclinicity. As the coastal deformation is strengthening, the onshore flow evolves to slantwise circulation favorable for the formation of cloud bands and/or rainbands that have been recognized as being a result of conditional symmetric instability (Bennetts and Hoskins, 1979; Emanuel, 1983). Hence, the induced mesoscale flow is highly variational with frontal deformation and cloud development. Since the coastal front represents a thermal boundary, pollutant transport and diffusion as influenced by the frontal dynamics will become rather complicated. In addition, cloud updraft with vigorous buoyancy during frontal formation may play a significant role in redistributing upper-level pollutants if they have been diffused into clouds.

The present study will rely on a mesoscale numerical model and will focus on the dynamical processes controlling pollutant redistribution. The sink effects such as dry and wet depositions and other removal processes will not be considered at this stage. We will briefly introduce the numerical model in Section II. Simulation results from a number of control numerical experiments conducted in this study are discussed in Section III. Further highlighted discussions with relevance to some key factors and source height and emission time are given in Section IV. A conclusion is provided in Sections V.

II. The Numerical Model and Case Experiments

1. The Numerical Model

The mesoscale numerical model used in this study is the same with that in Huang and Raman (1992) except that a mass-conservative equation for pollutant concentration has been included. The model is hydrostatic and anelastic in a terrain-following coordinate system. The model physics includes cloud microphysics that basically follows Kessler's formulations (Kessler, 1969). To account for horizontal advection, a modified version of the Warming-Kutler-Lomax (WKL) advection scheme is used. The performance of this modified scheme is nearly identical to that of the fourth-order leapfrog scheme, but the former saves considerable computer memory because of its two-time-level feature (Huang and Raman, 1991c). More important, this scheme performs much better for positive definite scalars since it employs a free parameter to control numerical dispersion and dissipation more effectively. In the vertical, the second-order Crowley advection scheme is employed because of its large time step for numerical stability. Time-splitting has been used for each directional advection; thus, gross numerical stability is assured based on the stability of each scheme.

A turbulence closure scheme based on two prognostic equations, one for turbulence kinetic energy (TKE) and the other for turbulence energy dissipation (ε), is incorporated with the level 2.5 formulation of Mellor and Yamada (1982) to determine eddy diffusivity (Huang and Raman, 1991a). This modified E-ε closure model has been shown to be reliable in boundary layer simulation (Huang and Raman, 1991a,b). All vertical diffusion terms are computed by a time-implicit scheme that allows the model to use a time step that is not constrained by turbulent diffusion (Huang and Raman, 1988).

The prognostic mass-conservative equation for air pollutant concentration includes advection terms and the subgrid vertical turbulent diffusion term. Subgrid horizontal diffusion terms are neglected since these terms generally reduce the amplitude preservation of concentration. Eddy diffusivity for heat from the turbulence closure model is used as the vertical eddy transfer coefficient for concentration.

2. The Case Experiments

In this study, we will limit ourselves to 2-D cases despite the fact that 3-D cases have been simulated by the model (Huang and Raman, 1992). This enables us to use much higher horizontal and vertical grid resolutions in more cases. Another important reason is that coastal frontal circulation will be essentially two-dimensional if both the coastal baroclinicity and coastline are primarily lined without large curvatures (Huang and Raman, 1992). This assumption of two-dimensionality, however, inevitably requires not only an uniform

coastline but also a lengthy emission source in the third direction.

There were totally eleven case experiments conducted in this study. A detailed description of these numerical experiments is given in Table 1. Most of the experiments were sensitivity tests. As expected, many physical parameters may be involved in the structural determination of the coastal circulation. However, we prefer to focus on the effect of frontal formation on pollutant diffusion and transport; thus, cases with onshore ambient flow are particularly considered in this study. Offshore ambient flow has been found to exhibit an offshore moving circulation front as typical breeze fronts; hence, it tends to diffuse and transport the pollutants away from the coastal region and should have less impact on the inland environment. The contents of inland moisture may also play a significant role although low-level moisture over ground during the formation of a coastal front often is dry as compared to daily breeze conditions. Another key parameter is the magnitude of onshore ambient wind speed. The cases should include the shear condition since it not only introduces atmospheric baroclinicity but also changes the low-level wind speed. Previous numerical studies (Huang and Raman, 1991b) indicated that the front is much more sensitive to wind speeds at low levels than at upper levels. Stronger low-level ambient flow also tends to suppress the development of coastal frontal circulation. Thus, we may anticipate that different ambient wind profiles will produce dramatically different structures of mesoscale coastal circulation and, thus, pollutant distributions.

Another important parameter that can be intuitively expected is the existence of mountain barriers in the coastal region. Many coastal polluted cities are known to be situated nearby small or high mountains and usually have worse air quality than plain cities do. For example, the city of Los Angeles in basin terrain is troubled by photochemically-induced pollution which is believed to be primarily caused by trapped pollutants which provide acting aerosols. The mountain influence on the geometric distribution of air pollutants appears to be important for apparent pollution problems and is worthy of investigation.

The model initialization follows our previous studies and the details can be found in Huang and Raman (1992). Initially, the flow is assumed to be horizontally homogeneous and to be heated up by the warmer sea surface water. The initial relative humidity (RH) is also assumed to be constant over the model domain. As the coastal front develops, the inland mid-level atmosphere can become more moist because of the onshore maritime flow penetration. The initial ground temperature is set to 10°C, and the far offshore sea surface temperature is assumed to be 25°C uniformly with a short transition zone set on near-coastal girds. Note that the large initial temperature difference between the ground and sea surface water may apply to some winter cases, but it is intended practically for triggering frontal formation near coasts. A neutral surface layer with zero sensible heat flux is assumed over ground. Over water, turbulent heat fluxes in the surface layer are determined by available similarity theory. The total numerical simulation time is 36 h with a uniform horizontal resolution of 5 km. There are totally 120 horizontal grids and 36 vertical grids.

Table 1. Two-Dimensional Case Experiments* Conducted in This Study. The Last (Right) Column Indicates Extreme Values in the Model Domain during the Simulation Time

Case	Descriptions of Experimental Parameters	[u_{min}, u_{max}, w_{min}, w_{max}]
U1	U_g=−1 m/s, RH=50%.	[−5.69, 6.53, −0.13, 0.81]
U1R8	U_g=−1 m/s, RH=80%	[−9.72, 11.69, −0.36, 1.76]
U2	U_g=−2 m/s, RH=50%.	[−6.68, 4.76, −0.09, 0.31]
U2R8	U_g=−2 m/s, RH=80%.	[−9.29, 6.30, −0 27, 1.01]
U2S4	U_g=−2 m/s, $\partial U_g/\partial z$=0 004 s^{-1}, RH=50%.	[−3.76, 46.75, −0.25, 0.48]
U4	U_g=−4 m/s, RH=50%.	[−6.89, 3.10, −0.06, 0.22]
U4R8	U_g=−4 m/s, RH=80%.	[−6.97, 2.98, −0.06, 0.22]
U4S4	U_g=−4 m/s, $\partial U_g/\partial z$=0.004 s^{-1}, RH=50%.	[−7.10, 44.70, −0.62, 1.43]
U4M1	U_g=−4 m/s, RH=50%, h_m=200 m, S=3 Δx, 100 km west of the coastline, instantaneous lifting.	[−6.94, 3 66, −0.06, 0.24]
U4M1H	U_g=−4 m/s, RH=50%, h_m=500 m, S=3 Δx, 100 km west of the coastline, instantaneous lifting.	[−9 11, 13.98, −0.24, 0.23]
U4M2	U_g=−4 m/s, RH=50%, h_m=1 km, S=5 Δx, 200 km west of the coastline, one-hour lifting	[−12.6, 4.77, −0.42, 0.29]

* All cases employed the Coriolis parameter f at latitude 25 °, stability stratification N~0.01 s^{-1}, and sea surface temperature (SST) gradient 15°C/25 km with Δx=5 km and Δt=30 s for 36 hour simulation. The last three cases imposed a Gaussian mountain $h=h_m \exp(-x^2/S^2)$ where h_m was the central maximum height

The coastal baroclinicity possesses a 15°C variation of sea surface temperature within a distance of 25 km (from grids 80 to 85). Sea surface temperatures are unmodified during the numerical simulation time. The simulated ambient environment is set at moderately stable conditions with the gravitational stability parameter N~0.01 s^{-1}.

In this study, we will consider only instantaneous sources. An area source is located on inland grids 76 to 80 in the layer of the lowest 50 m and is released at the initial time. The initial pollutants within the source region are assumed to be well mixed with a uniform magnitude of 100 units. The block structure of the pollutant distribution for the diffusion processes may also imply that the concentration indeed gradually decays to zero at the adjacent grids; thus, the occupied region of the pollutants is increased. A lower boundary condition of total reflection (i.e., no surface flux) for the pollutant concentration is thus assumed for simplification.

III. The Case Results

1. A Systematic Overview

Before discussing detailed pollutant distributions, we should take a systematic look at the development of the coastal circulation. The developed extreme values of the wind speeds for u and w during the simulation time were recorded and are given in Table 1. As can be seen in this table, an increase in RH led to significant amplification of the circulation updraft. For weaker flow (Cases U1 and U1R8), this effect was more pronounced. As the flow became stronger, the increase in RH seemed to have little effect, however. Another interesting result was that the wind shear did not cause similar effects among the cases. For example, the updraft for the shear case U4S4 was much stronger than that for the corresponding nonshear case (U4). This intensification was not apparent for the two cases with weaker flow (U2 and U2S4). Finally, we see that the last three cases with a mountain barrier included did not have significant discrepancies in coastal updraft development.

Time evolutions of the domain maximum and minimum vertical velocities are plotted in Fig. 1 for selected cases. As can be seen in this figure, the updraft for U1R8 in general was strongest during system development. Again, reduction in RH (Cases U1 and U2) led to a much more slowly developing updraft. Development of the updraft in the weak dry flow required a larger integration time than in the moist flow as can be seen in the U1 results. Thus, it is clear that the profile of inland moisture above the PBL was significant for system development with weak ambient flow. For stronger ambient flow, the system intensity did not significantly increase due to the increase in RH. Indeed, there were no noticeable differences between the U4 and U4R8 results (Fig. 1c).

In the case results of U1R8, one can clearly identify an instability associated with the updraft during its earlier development time between 10 h and 20 h. This instability was very weak for the dry case, however. As found in Huang and Raman (1992), such instability in U1R8 was caused by the developing slantwise circulation that could release conditional symmetric instability (CSI). For strong ambient flow, CSI did not occur as in U4R8 and indeed no intense updraft was found in this case. However, CSI did appear in the shear case (U4S4). In the latter case, the updraft ceased to grow and became weaker with time after the period of the peak updraft intensity. This characteristic feature was due to the fact that the updraft had moved out of the model domain at later times. As will be shown later, a case with offshore wind shear of ambient flow may exhibit an offshore penetrating front rather than a quasi-stationary front in the vicinity of the coast.

The systematic overview provides some important information. First, the coastal frontal circulation took about a half day or so to develop. The length of the spin-up time partially depended on the initial RH. Second, the intense circulation updrafts tended to appear in coexistence with CSI, indicating a role of latent heat release in the frontal flow. Third, the wind shear had some effects on system development, but its broad influence is not immediately clear at this point. Finally, the mountain barriers imposed for different cases seemed to have a secondary role in the development of coastal updrafts (Fig. 1d). However, the coastal pollutant transport and diffusion in fact could be significantly influenced by the mountain barriers.

2. Geometric Distributions of Clouds and Pollutants

One of our primary focuses was on the distribution of the modeled clouds that were associated with weaker stratification and were, therefore, favorable for further transport of pollutants and enhanced diffusion. However, the pollutants could by distributed without any correspondence to the cloud field as will be seen later. The cloud formation was greatly related to the development of the coastal front where the mature or intense updraft was present during frontogenesis. Formation of the coastal front can be clearly seen in Fig. 2 for Case U1. The major updraft at 12 h appeared just right of the eastern boundary of the sea-surface temperature variation. It mainly followed the frontal isentropes and

then became a downward motion. Behind (west of) the leading front (gird 85), there was flow acceleration near the surface. This was a typical near-surface jet as is often found in intense breeze fronts and was caused by the wind adjustment to the induced pressure perturbation due to differential boundary layer modification over the coastal baroclinic zone. Because of the near-surface offshore jet, a number of the pollutants were carried away from the initial source location (grids 76 to 80) as the coastal front was developing. As can be seen, some pollutants mainly followed the frontal circulation, thus reaching the height of the upper frontal

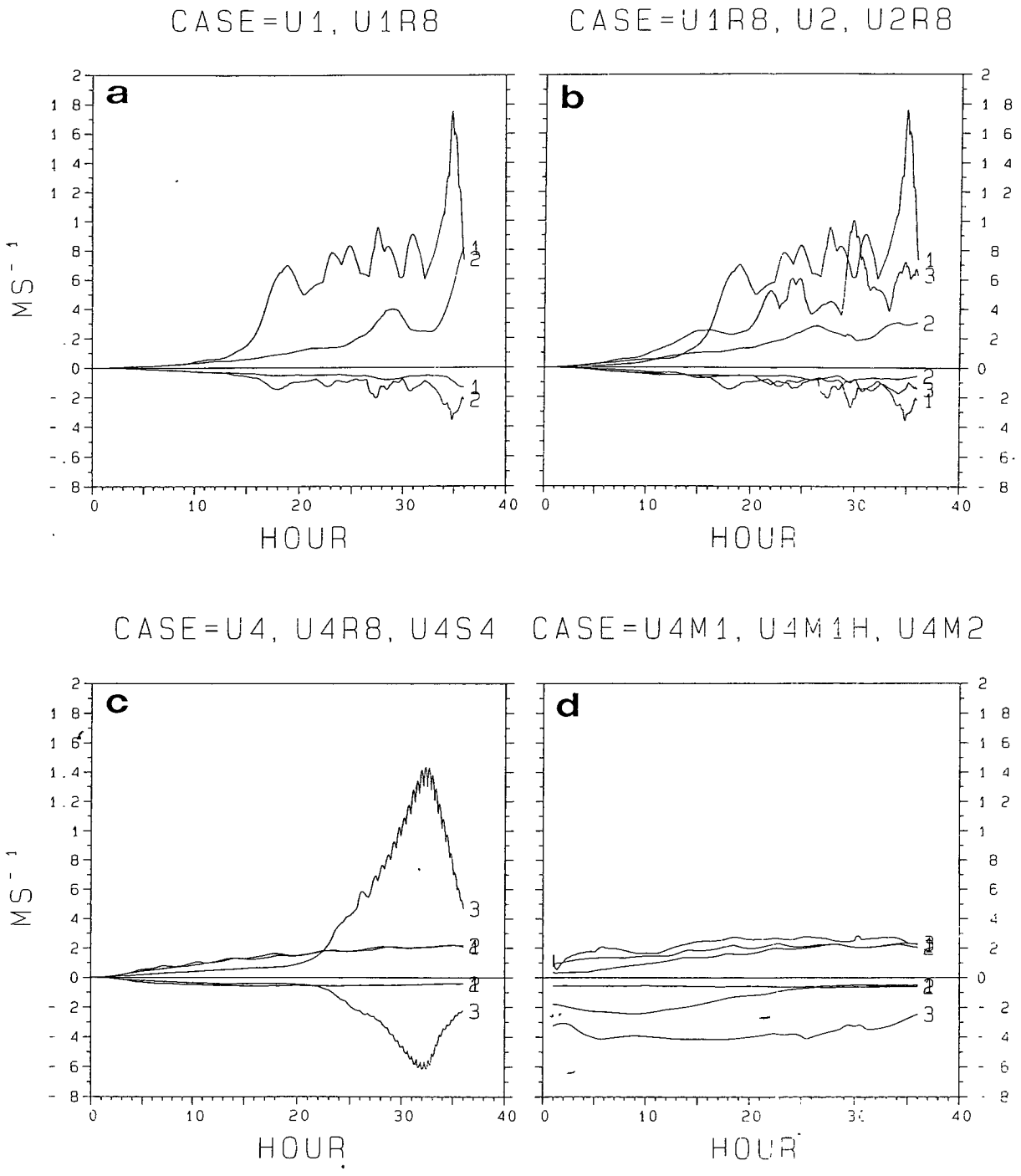

Fig. 1. Time evolutions of maximum and minimum vertical velocities in the model domain. (a) Cases U1 (denoted by 1) and U1R8 (denoted by 2); (b) U1R8 (1), U2 (2) and U2R8 (3); (c) U4 (1), U4R8 (2) and U4S4 (3); (d) U4M1 (1), U4M1H (2) and U4M2 (3).

surface. For this case with weak ambient flow, the marine boundary layer (MBL) developed to about a 1 km height at 12 h and continued to grow, but slightly, with the simulation time. The height of the coastal front was closely related to the developed MBL height.

Keep in mind that there was near-surface onshore ambient flow initially for all the cases in this study. In Fig. 2b, one thus can see that the leading pollutants moved further inland to about grid 69 at 24 h. At a later time when the near-surface jet further strengthened, the pollutants were blocked to the west and were diffused more vertically because of the reduced stratification. The region of this weaker stability was associated with the onshore upper-level outflow of the frontal updraft. At 36 h, the geometric distribution of the pollutants above the frontal surface resembled the cloud distribution very well. It appears that the anvil was responsible for the similarity in the pollution for this case. Pollutant transport was essentially similar to the moisture transport in the clouds. The dynamical features of the intense cloud formation for similar coastal fronts were discussed by Huang and Raman (1992). It is interesting to see that diffusion processes dominated advection processes at low levels, particularly in the MBL over the ocean. Thus, the pollutants became well mixed within the boundary layer at later times as compared to 12 h (Fig. 2a). The advection effect, however, moved the pollutant pattern and thus determined the horizontal spreading of the pollution through flow divergence.

Note that there were some two-grid-interval (2-Δ) wavy patterns of the concentration in the region of

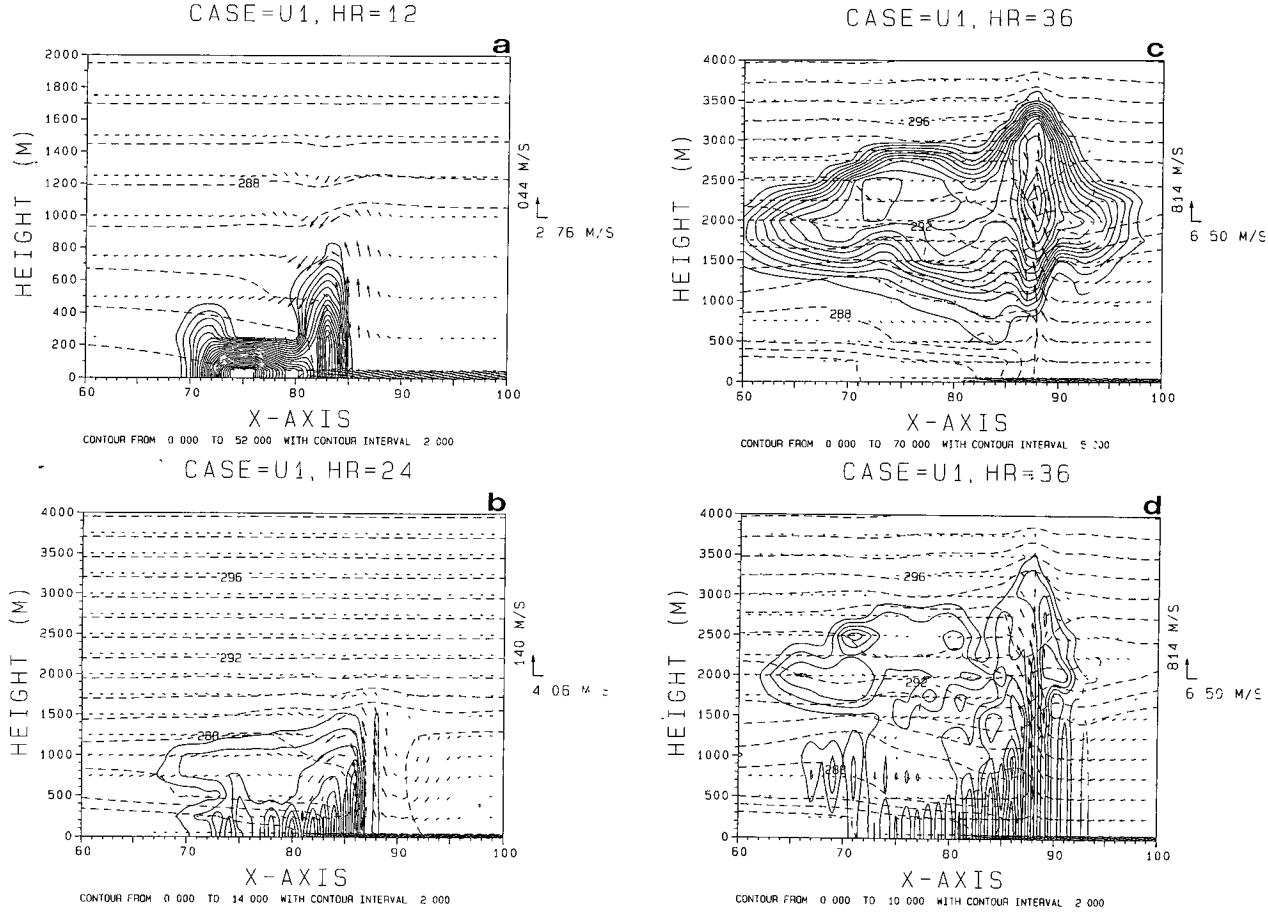

Fig. 2. The numerical results for Case U1. (a) Concentration at 12 h; (b) concentration at 24 h; (c) cloud water at 36 h; (d) concentration at 36 h. In the figure, dashed lines are for potential temperature with a contour interval of 1 K, and the wind vectors for u and w velocities are also plotted with their maximum magnitudes to the right of each panel. The contour intervals are 2 units for concentration and 0.05 g kg^{-1} for cloud water. Contour configurations are also indicated below each frame. The coastline lay on grid 80 and the surface layer pollutants were released over grids 76-80 at the initial time.

frontal convergence as seen in Fig. 2 (these features are also present in some later results). These patterns that were more apparent at later times resulted from the modified fourth-order Crowley advection scheme which generally preserved amplitude very well but would lead to noticeable shortwave dispersion after long-term integration as the advecting flow was rather deformational. Normally, the modified Crowley advection scheme is much more reliable than the unmodified versions as applied to advection of a positive-definite scalar field as found by Huang (1993, 1994) and is effective in controlling the dispersion of 2-Δ waves provided that the flow is not strongly deformational and that the initial concentration field is rather smooth without a large component of 2-Δ waves. (In our cases, the initial concentration field was a long horizontal box with sharp gradients.) The wavy structures could be smoothed out if a linear filter for 2-Δ waves or the horizontal diffusion terms (for the formulation, see Huang and Raman, 1988) were employed in the concentration calculation or if more diffusive positive-definite advection schemes (e.g., the first-order upstream scheme) were used, but the reduction in the maximum concentration was found to be considerable. In all the cases above, the gross patterns of the concentration redistributions were similar despite the presence of low-level 2-Δ wave dispersion. (Hence, the simulation results are not shown herein for brevity.) Better high-order positive-definite advection schemes possessing little dissipation and good phase are demanding for modeling such cases with strong frontal deformation, but to date such schemes exist only in a flux form for constant grids. In our case simulations, the vertical grids near the surface were highly stretched, and the governing equations are featured with the advection terms in an advective form.

Figure 3 shows the case results of U1R8. In this case, initial RH was uniformly set to 80%, which was increased from 50% in Case U1. The effects of additional moisture contents were apparent as the results show that the circulation was much stronger than that for the lower-RH case (also see Fig. 1). At 24 h, clouds were produced up to a 4 km height, and the major updraft (near grid 88) was much stronger than was that for U1. Because of the intense coastal frontogenesis, the pollutants were forced to move offshore and to undergo diffusion over the coastal water. As where, the pollutants were well-mixed by strong turbulent diffusion in the MBL. Some of the vertically diffused pollutants were carried further upward, essentially following the penetration of the frontal updraft. Above the boundary layer, the pollutants resembled the clouds in distribution as found in the U1 results.

As the easterly onshore ambient wind speed was

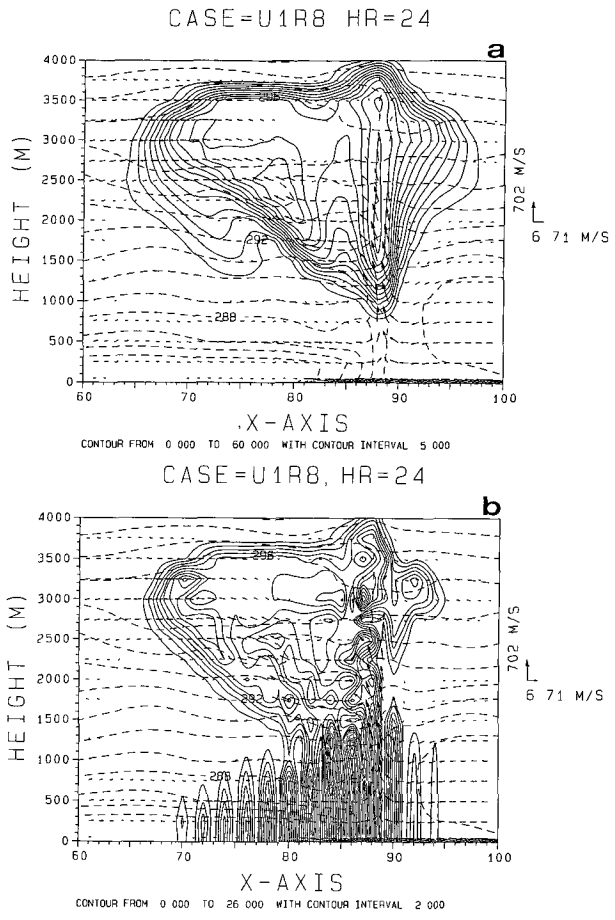

Fig. 3. Same as Fig. 2 but for Case U1R8 (with increased uniform RH of 80%).

increased to 2 ms^{-1}, formation of the coastal front still appeared. The location of the coastal front was somewhat closer to the coastline as compared to the results of Case U1 (Fig. 4). Some of the pollutants moved further inland to about grid 47. Some were vertically transported and redistributed following the cloud pattern, and the other pollutants penetrated offshore and became well-mixed in the MBL. Comparing Fig. 4b to Fig. 2b, one can see no significant discrepancies between the pollutant patterns for the two cases of U1 and U2, except that the leading pollutants for the latter case moved further inland since they escaped the domination of the developed near-surface offshore jet.

The case results of U2R8 (with increased RH of 80%) are shown in Fig. 5. As indicated in Fig. 1, the increase in RH greatly intensified the system development. For example, the strongest upward motion in the moist case increased to 1.01 ms^{-1} from 0.31m s^{-1} in the dry case. Higher RH also led to an earlier onset of system development with the near-surface offshore jet forming further inland. The inland pen-

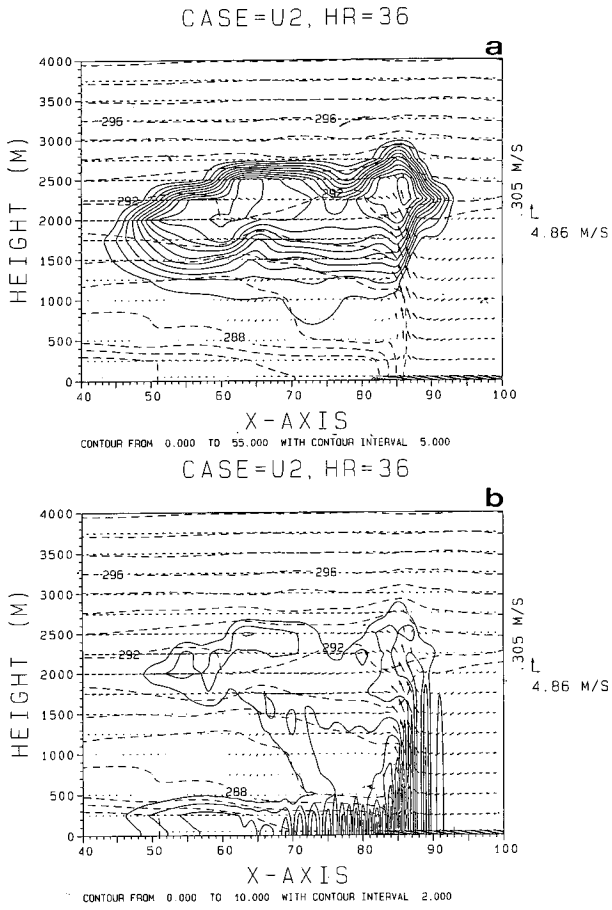

Fig. 4. The numerical results for Case U2. (a) Cloud water at 36 h; (b) concentration at 36 h. Other plot information is the same as in Fig. 2.

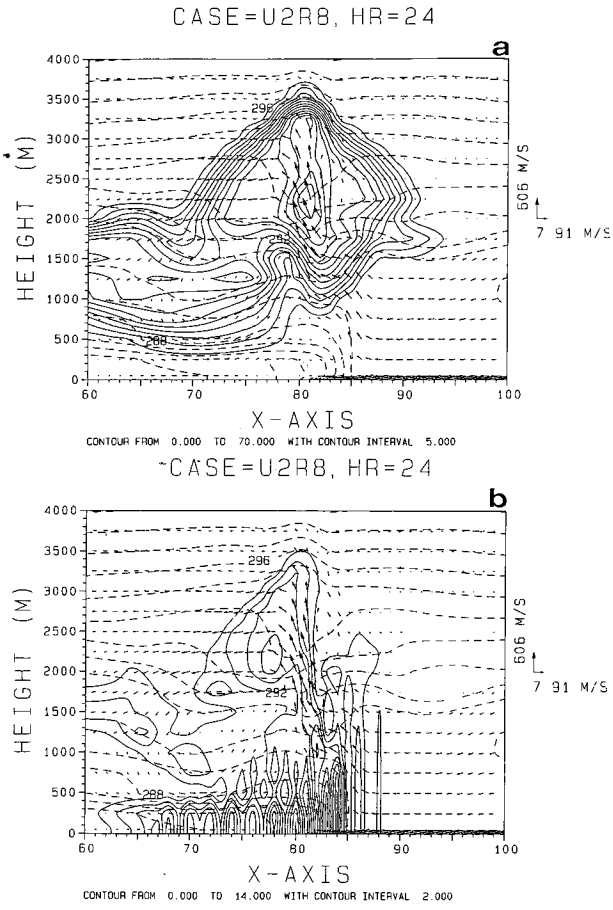

Fig. 5. The numerical results for Case U2R8 (with increased uniform RH of 80%). (a) Cloud water at 24 h; (b) concentration at 24 h.

etration of the pollutants was resisted by the near-surface jet which developed later as can be found in the results at 24 h (Fig. 5b). As the coastal circulation became stronger, the low-level onshore flow following the low-level frontal lifting experienced a second uplifting over the surface front. This feature has also been found in some cold-front cases (e.g., Knight and Hobbs, 1988). It indicates that the inland higher RH facilitates a second saturation condition for the upper-level onshore outflow of the frontal updraft.

The cloud formation near the coast was further enhanced by the near-surface offshore jet that partly fed into the outflow of the first penetrating frontal updraft (Fig. 5b). As the initial RH increased, this coastal flow convergence at upper levels led to formation of a stronger (second) updraft compared to the one in the MBL. Strong onshore outflow at higher levels was caused by the divergence of the second updraft at a height of the penetrative depth. As a consequence, the upper-level pollutants were transported to higher levels and deeper inland regions following the second updraft and outflow. The pollutant concentration, however, was greatly diluted because of the increased spreading regions, and it was less than that for the dry case. In fact, a big discrepancy between the gross patterns of the pollutants for the weak flow cases (U1 and U1R8) and the stronger flow cases (U2 and U2R8) can be clearly identified. The pollutants were present primarily west of the coastal front for the latter cases, but their distribution was rather symmetric about the coastline for the former cases.

As the ambient wind shear was present in these cases, the pollutant patterns may have been quite different from those where no shear was included. Figure 6 shows the case results of U2S4. In this case, the ambient flow was onshore at low levels but became offshore above 500 m. At 12 h(not shown), the structure of the frontal circulation was similar to that for the nonshear case since the front remained shallow. As the coastal frontogenesis further intensified, the shear

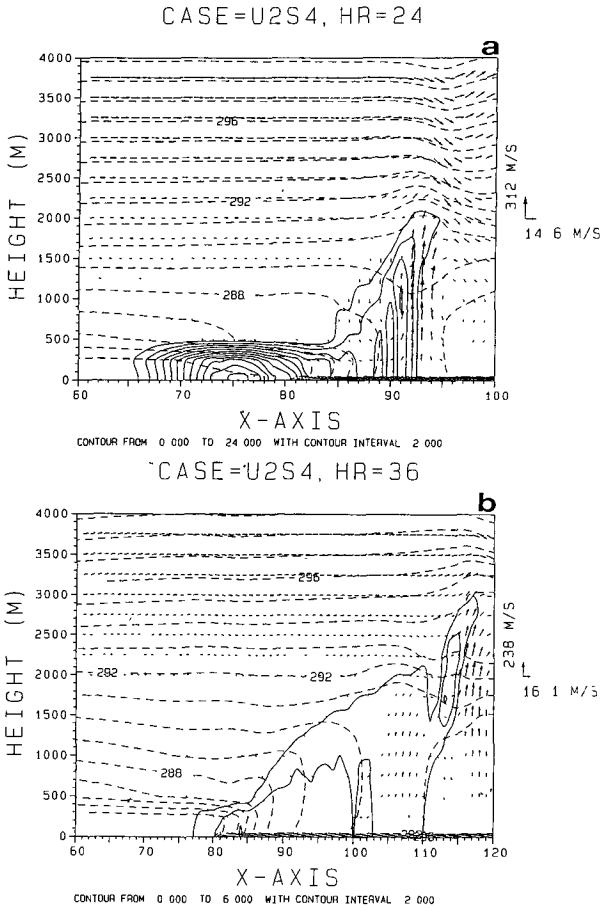

Fig. 6. The numerical results for Case U2S4 (with the shear of 0.004 s^{-1}). (a) Concentration at 24 h; (b) concentration at 36 h. Other plot information is the same as in Fig. 2.

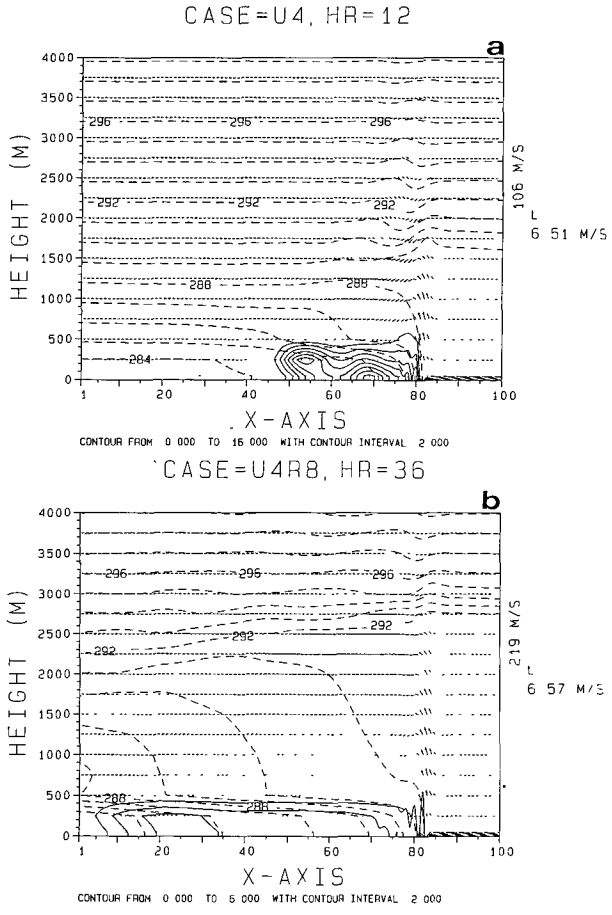

Fig. 7. The numerical results show (a) concentration at 12 h for Case U4 and (b) concentration at 36 h for Case U4R8. Other plot information is the same as in Fig. 2.

effects became more apparent. The front, indeed, moved slightly offshore as can be seen in this figure. Some of the pollutants thus were brought offshore away from the source region and then were redistributed upward by the frontal updraft in further offshore regions. Over the ground, the pollutants were situated within the shallow layer of the lowest 500 m and were weakly advected inland by the light easterly wind as can be seen at 24 h (Fig. 6a). Because of the movement of the offshore developing front, most of the pollutants were slowly advected offshore with the increasing diffusion (Fig. 6b).

Similar to breeze fronts, coastal fronts are sensitive to the intensity of ambient winds. This is illustrated in Fig. 7 for Cases U4 and U4R8. As indicated in Fig. 1, these two cases had almost same results, implying that the increase in RH did not have a significant role in the case of stronger ambient flow. At 12 h, the frontal updraft appeared near grid 82 and was much closer to the coastline than was that for the case of weaker wind. All of the pollutants were distributed inland, indicating that the near-surface offshore jet was very weak for this case and was present only near the coastline at this time. At 36 h, the leading pollutants had moved deeply inland to grid 5. It is interesting to see that the pollutants were diffused within the lowest layer of 500 m above which the potential temperature field had been greatly modified due to loss of its originality because of the onshore penetration of the maritime flow.

The nonshear cases (U4 and U4R8) clearly exhibit a noticeable feature of the frontal deformation. As can be seen in Fig. 7b, the low level of the front (below 500 m) remained similar to that for Case U2, but the upper level of the front tilted inland because of the strong onshore flow penetration. No detectable clouds were produced for this case even though the virtual potential temperature field showed that a moisture

tongue had intruded into the western boundary of the model domain (not shown). Compared to the low-level coastal front, the inland upper-level flow structure over the front possessed much weaker baroclinicity and stability. Below this weaker stability layer over the land, there was a thin stable layer just above the assumed near-surface neutral layer. Since almost all of the pollutants were trapped below this stable layer, advection processes apparently dominated diffusion processes for the pollutant redistribution.

The characteristic features of the frontal circulation for the other shear case U4S4 with stronger near-surface ambient onshore flow were significantly different from those for the nonshear cases U4 and U4R8. The case results of U4S4 are shown in Fig. 8. The earlier patterns of the front and pollutants (e.g., at 12 h) were similar to those for the nonshear cases. Only slight offshore movement of few pollutants was caused by the near-surface offshore jet despite the fact that the ambient flow was onshore at low levels. At 24 h, almost all of the pollutants moved further inland but remain diffused within the lowest 500 m height except for one peak concentration appearing offshore near grid 86. The presence of this peak concentration, though being not significant because of its small magnitude, is a good illustration of the advection-diffusion processes. As a small amount of the pollutants were impelled to the oceanic region by the near-surface offshore flow, they could be well-diffused within the MBL and also transported upward by the frontal updraft. This combined effect resulted in the presence of the light columnar concentration.

The leading pollutants reached grid 20 at 36 h for the shear case U4S4, with a moving speed slower than that for the nonshear case U4R8. This can be explained by the counteracting effect of the offshore wind shear. One of the striking features for this case is that the circulation exhibited offshore development despite the fact that the low-level ambient wind was onshore. The developed height of the MBL was about 1.5 km or so. It should be noted that the ambient wind vanished at 1 km height and became offshore at a speed of 4m s^{-1} at 2 km height. Within 12 h (24-36 h), the frontal updraft moved from grid 88 to grid 110, traveling a

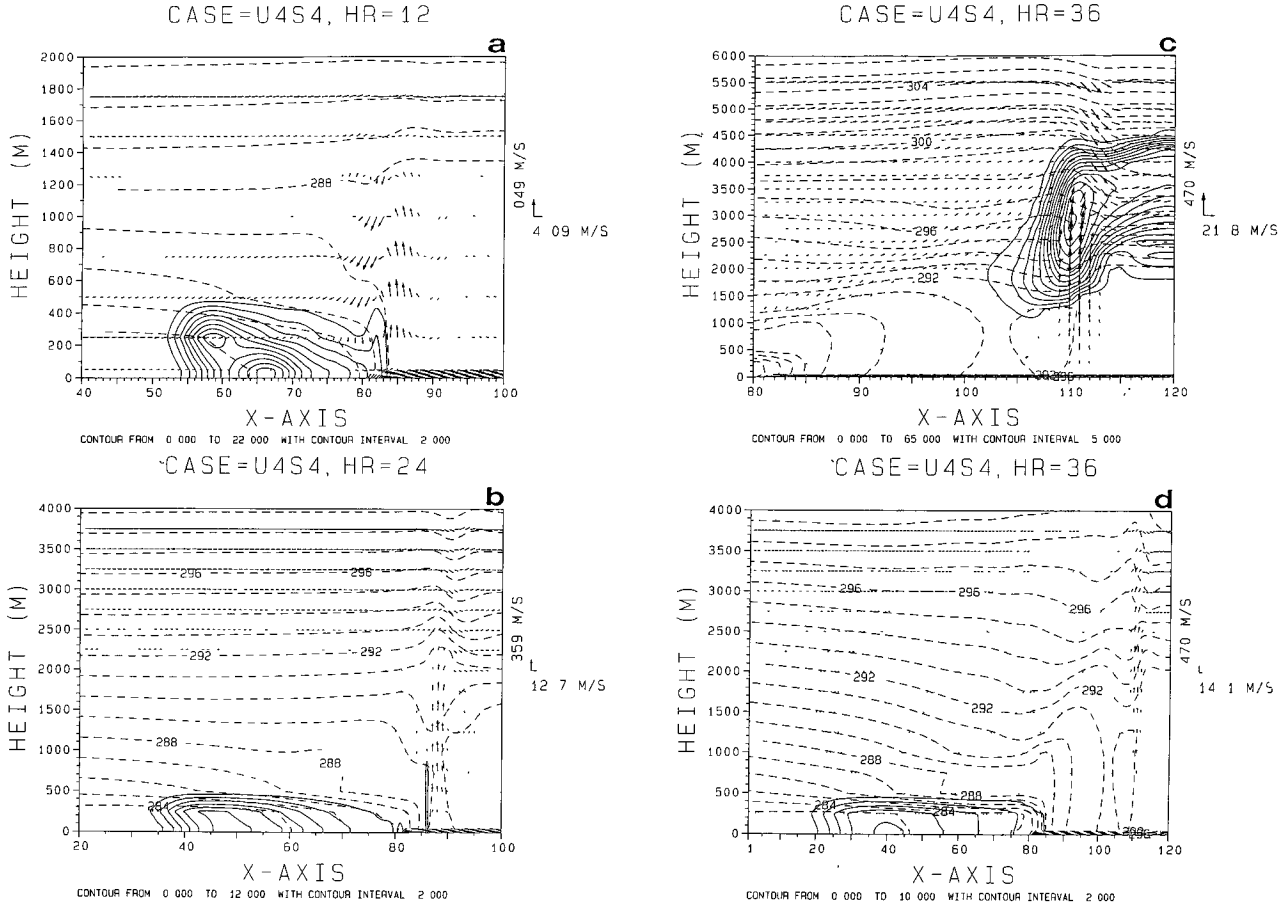

Fig. 8. Same as Fig. 2 but for Case U4S4.

distance of 110 km. This indicates an average moving speed of 2.54 ms^{-1}, which corresponded to the ambient wind speed at a height of 1.63 km. Thus, the movement of the coastal front was at the characteristic speed of the ambient wind at the MBL height, although the incipient development of the front was dominated primarily by the near-surface ambient flow.

It is easier for air pollutants to be confined in light-wind conditions; hence, reduction of pollution must rely on the efficient vertical (and lateral) diffusion. Bad ventilation often causes severe pollution as a result of calm winds and feeble turbulence. As the wind becomes stronger, pollutants are expected to move with the wind more swiftly. Since the wind field may be deformational and variational in the coastal frontal circulation, the pollutants are redistributed in a complicated way. Nevertheless, the previous case results have clearly demonstrated the effects of stronger wind speed in enhancing the inland transport of pollutants except when the offshore ambient wind shear is present to drastically change the direction of the mesoscale circulation.

Because of the lateral movement and spreading effects, the concentration of the coastal pollutants can be expected to be greatly reduced in the source region. The pollutants can be either diffused more vertically or transported more widely for a reduction of the near-surface maximum pollution. As mentioned before, these natural processes (advection and diffusion) often are countered by the presence of terrain barriers such as mountains. For example, most of the pollutants felt no blocking effect in the case U4M1 as a small hill (200 m height) was imposed 100 km west of the source location (Fig. 9a). This can be seen by comparing Figs. 7a and 9a. However, they become significantly impeded east of the hill where the central height increased to 500 m (Fig. 9b).

The hill 200 m high in the U4M1 case was lower than the top of the stable layer. For mountain flow, the Froude number can be defined as $Fr=U/Nh_m$, where U represents the characteristic speed of ambient flow, and h_m is the maximum terrain height. This number can be considered as the ratio between the kinetic energy and the potential energy and is indicative of the flow behavior in confrontation with an obstacle. The Froude number is 2.0 for U4M1. According to linear theory (Smith, 1979), the flow should swiftly pass over the hill as can be seen in the case results of U4M1. As the Coriolis effects are involved, the Rossby number ($Ro=U/fL$ where L characterizes the length scale of the flow) also plays a part in influencing the flow behavior. Based on the nonlinear simulations which were designed to construct the relationships between the upstream influence and the two parameters Ro and Fr,

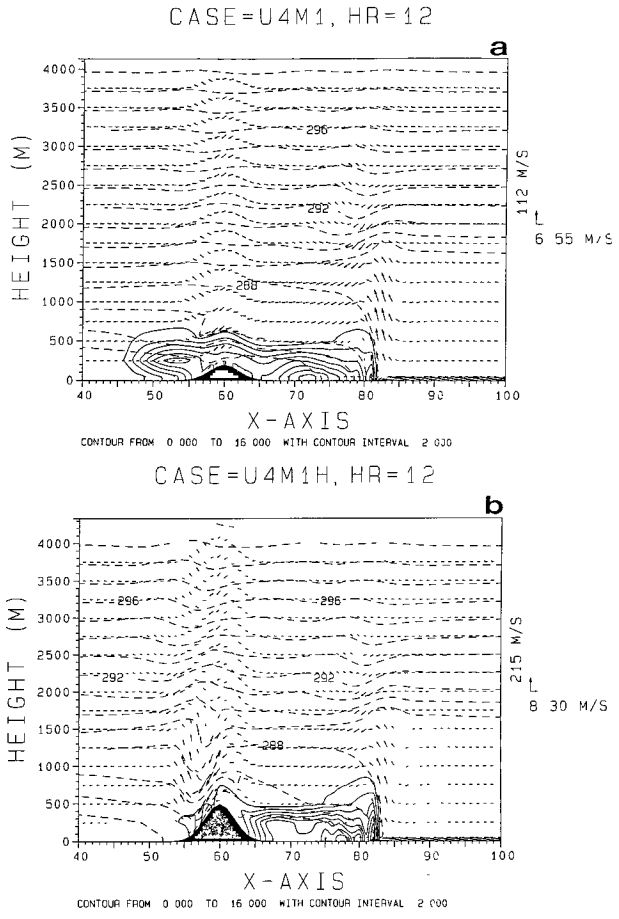

Fig. 9. The numerical results show concentration distributions. (a) 12 h for Case U4M1, (b) 12 h for U4M1H.

Pierrehumbert and Wyman (1985) indicated that for a mesoscale Gaussian mountain upstream influence would cause the inviscid near-surface flow to stagnate for $Fr^{-1}>1.5$ in nonrotating systems. The presence of the Coriolis effects tends to force the flow to adjust to the geostrophy. Hence, the upstream blocking zone if it exists is retreats toward the obstacle with time. The actual phase and location of the flow stagnation is also significantly related to the Rossby number. In the case of U4M1H with the higher hill (500 m), the Froude number fell to about 0.8 for the uniform onshore ambient flow and indeed could be smaller because of the boundary layer friction and the development of the offshore near-surface jet involved in our cases. This indicates that the near-surface flow should experience marginal blocking or prominent deceleration for the case U4M1H. However, some of the pollutants near the coast if diffused to levels higher than the critical height (say about 170 m despite more or less modification due to boundary layer effects) could accordingly still be carried over the 500 m height mountain. In

fact, the coastal pollutants were well-diffused within the MBL, and the flow that drove the pollutants possessed various Froude numbers. As a consequence, dense and lighter pollutions-resulted at the upstream and lee sides of the hill, respectively. The results indicate that the major of the pollutants blocked ahead of the mountain were input by the upstream low-level pollutants that were predominantly driven by the horizontal wind.

The upstream influence of the hill could be significant for the coastal flow because the distance of the hill to the coastline was only 100 km. In the case U4M2, the hill was moved 100 km further inland, i.e., 200 km away from the coastline. Further, the central height of the hill was increased to 1 km, and its half-width was also broadened to a factor of about 2. Thus, the Rossby deformation radius (Nh_m/f) was also doubled. Since the deformation radius is a measurement for the approximate scale of the mountain influence on the rotating flow, one could expect that the pollutant movement would be modified at further upstream locations for U4M2 despite the fact that the influence of coastal frontogenesis was also involved in the processes of pollutant redistribution. Figure 10 shows the case results of U4M2. Comparing Figs. 7a and 10a, one can see that the resisted pollutants changed in their leading position from grid 47 to 64 at 12 h due to the stronger influence of the larger hill. The coastal updraft also appeared about 2-3 grids further offshore at this time. In combination with the influence of the developed near-surface offshore jet near the coastal region, the blocking effect of the large mountain prevented the low-level pollutants from exceeding grid 70 by 24 h (Fig. 10b). For this case, stratus clouds formed from the coastal updraft region to the downstream side of the hill. This result was considerably different from that for the case where no hill was included. At 36 h, the leading pollutants at low levels remained near-stationary, but the pollutants in the vicinity of the coastal updrafts had been carried upward and inland, following the frontal isentropes. At upper levels, the wind was capable of blowing the pollutants over the hill as can be seen in Fig. 11a. It seems that the pollutants could be transported over the hill if they were diffused higher than 600 m high so that the relevant Froude number at this height was over unity. There was induced lee-side pollution in the cloud core in the layer 2-3 km high (Fig. 11a), indicating the involved buoyancy effects. However, the low-level parts of the pollutants were not influenced by the cloud dynamics. Indeed, the low-level pollution was mainly caused by the PBL diffusion processes (Fig. 11b), in addition to the transport of the strong downslope wind.

The 2-D modeling results for concentration

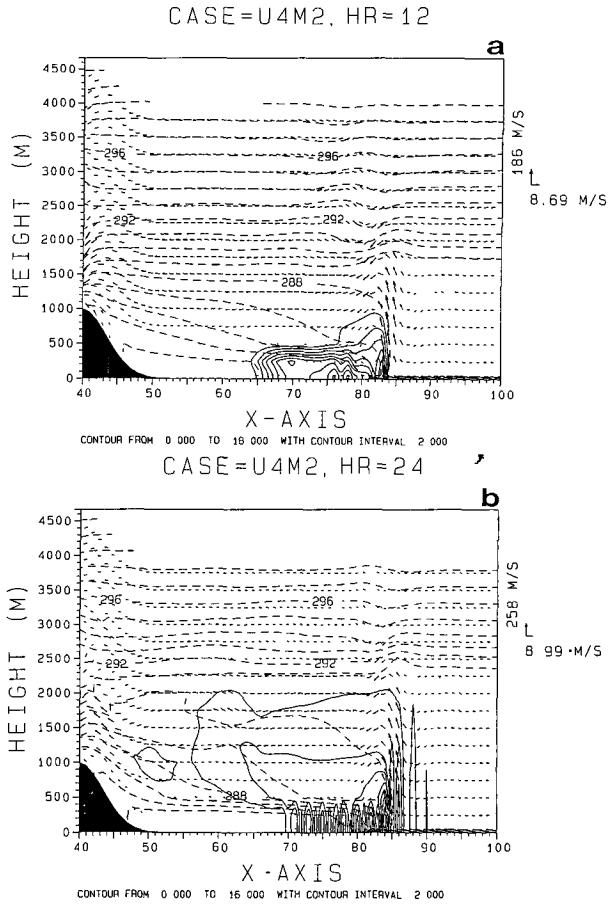

Fig. 10. The numerical results show concentration distributions for Case U4M2 at (a) 12 h; (b) 24 h.

near the mountain were basically valid as flow was rather symmetric about the y-axis, and the mountain was of the long-ridge type in the y-direction. In the 3-D cases, the flow could split around an obstacle and become recirculated or reverse at the lee side; hence, air pollutants impeded upstream of the mountain could re-enter downstream due to the 3-D flow field. It should be mentioned here that inclusion of 3-D fronts near the mountain in the model is believed to be a difficult task, and that the 3-D diffusion processes of air pollutants under uniform flow do not pertain to our goals.

IV. Discussion

1. Turbulent Diffusion

The redistribution of coastal pollutants is significantly related to the activity of turbulence, particularly at low levels. For purposes of illustration, Fig. 12

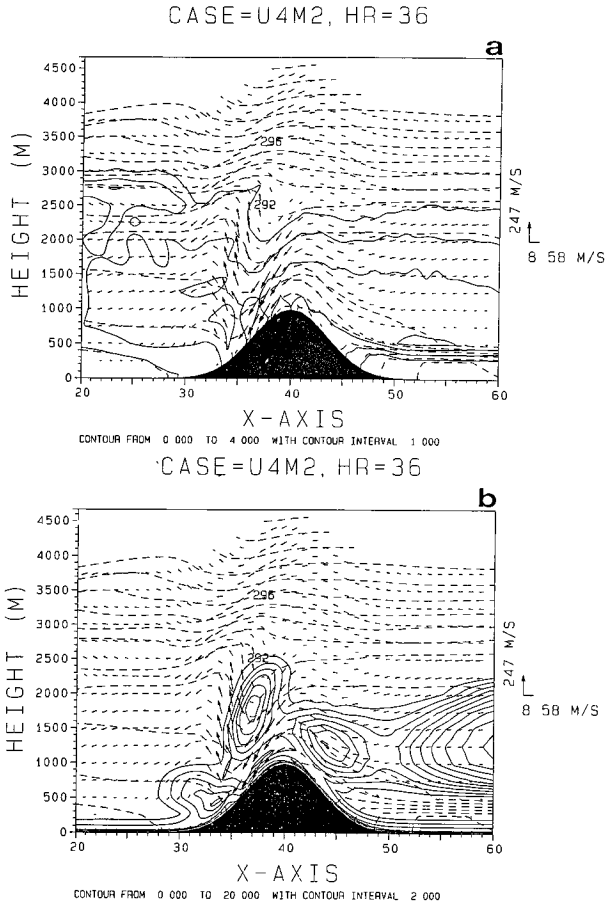

Fig. 11. The numerical results at 36 h for Case U4M2. (a) Concentration (unit); (b) eddy diffusivity for heat (m^2s^{-1}).

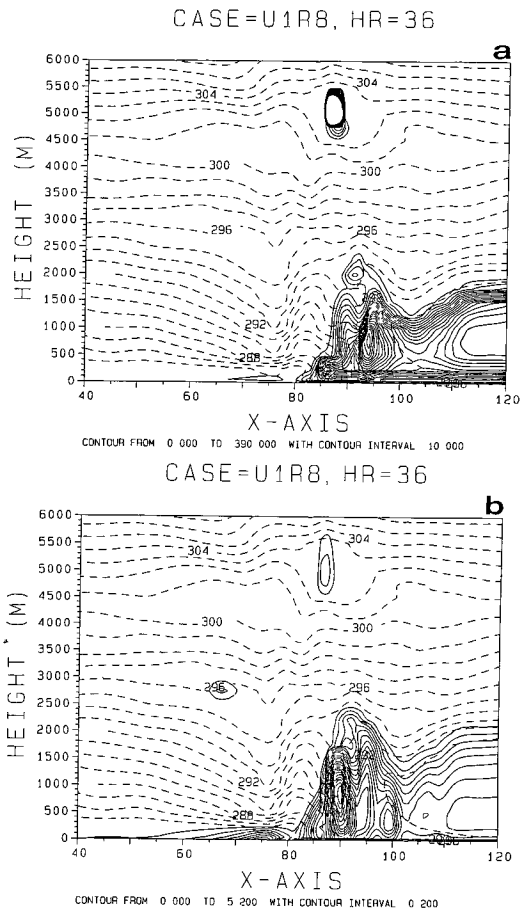

Fig. 12. The numerical results at 36 h. (a) Eddy diffusivity for heat (m^2s^{-1}) for Case U1R8; (b) turbulence kinetic energy (m^2s^{-2}).

shows the geometric patterns of eddy diffusivity and turbulence kinetic energy (TKE) for Case U1R8. The geometric distributions for these two fields were quite similar since the eddy diffusivity was parameterized by the TKE. The profile of eddy diffusivity for heat (K_h) over the ocean was typical of the convective boundary layer, showing a maximum near the middle of the MBL. At the location of the frontal updraft, the eddy diffusivity developed to a higher level in consistence with the MBL height that was somewhat larger than at other places.

It should be noted that there was a salient isolated region with maximum K_h near a height of 5 km where the cloud was very active as seen in Fig. 3a. This maximum value of K_h, however, was found to exceed 1200 $m^2 s^{-1}$, indicating a singularity that existed in the closure method of determining the eddy diffusivity. Our turbulence closure relies on a hybrid scheme of the level 2.5 and the E-ε closure model (for details see Huang and Raman, 1989). The level 2.5 has been known to exhibit singularities in some physical parameter spaces (Helfand and Labraga, 1988). It seems that the level 2.5 closure scheme is subject to singularities for a flow with strong shear in buoyant clouds. Despite the singularity for our modeling cases, the upper-level pollutant distribution (Fig. 3d) is reasonable and is very similar to the cloud pattern. Clearly, the upper-level pollution is caused by the cloud dynamics rather than the turbulent diffusion processes since only very weak eddy diffusivity is generated above the MBL. The well-mixed pollution at low levels over the ocean, in contrast, clearly indicates the domination of the turbulent diffusion processes. Over the ground, the eddy diffusivity is concentrated near the surface and, thus, diffuses the pollutants within this layer. As a consequence, the coastal pollutants near the surface are primarily redistributed by mean flow advection processes. There is no upward tendency of the pollutant transport over the ground.

2. Mean Transport

Mean transport is intimately influenced by variations in the velocity and stability of flow. The "mean transport" discussed here is referred to as the grid-scale transport of the flow. Previous figures have shown in great detail the mean transport features, especially the dispersion patterns within the convective circulation. Here, we are particularly interested in the effects of the flow variations due to mountain blocking during coastal frontogenesis since the results of the control experiments reveal the great importance of the mountain influence. As can be seen in Fig. 11 for Case U4M2, the low-level pollutants below the stable layer of the lowest 500 m were impeded east of the mountain top. Only pollutants originating at higher levels were able to pass over the mountain. As a result, the downstream side of the mountain was lightly and widely polluted. The pollution was related to the downslope wind transport and the turbulence activity induced by the effect of diabatic warming (Fig. 11b). Maximum TKEs were generated in the downslope region of the wind, indicating that the subgrid eddies were stronger there. In addition to the boundary layer generation, the TKE upstream of the mountain was also relatively stronger in the weak stability layer above the stable layer, reflecting the effects of the onshore maritime flow penetration. The existence of the pollutants above the stable layer may have been related to turbulence diffusion in this upper-level TKE generation. On the other hand, the pollutants could also have been advected by the wind from the diffused concentration at higher levels over the coastal region. There was wave-like distribution of the pollutants over the downstream side of the hill, in consistence with the tilting behavior of the mountain flow. Tilting indeed also existed for the TKE field on the downslope side. The wave-like patterns of the pollution and the flow, however, were destroyed near the surface. The results reflect the essential fact that the combined effects of mean flow and turbulence transport are rather complicated over the mountain region.

3. A Lagrangian View

In order to analyze pollutant transport more precisely for long-time transportation, a Lagrangian particle scheme was used to trace the pollutant movement due to mean flow advection. This trajectory analysis method has been adopted by many investigators (Anthes and Warner, 1978; Segal *et al.*, 1982). For our scheme, the velocity that actually drove the particle was estimated by values at neighboring grid points of the particle using quadratic interpolation. Three particles are distributed at the heights of 50, 500, and 1000m over grid 77, respectively. They were released at the initial time and at 12 h. Figure 13 shows the pathways of these three particles. Particle 1 (at 50 m height) first moved inland to about grid 73 and then turned back while Particle 2 (at 500 m height) moved much further inland to grid 50 and then stagnated there for a long time due to the mountain blocking. Clearly, the later offshore movement of Particle 1 was caused by the developed near-surface offshore jet as coastal frontogenesis greatly strengthened. As discussed previously, the particle at the height of 500m still could not pass over the mountain since the effective Froude number was slightly less than unity. On the other hand, Particle 3 experienced little mountain obstruction since it was released at a 1 km height. The pathway of Particle 3 also clearly reflects the characteristic feature of the

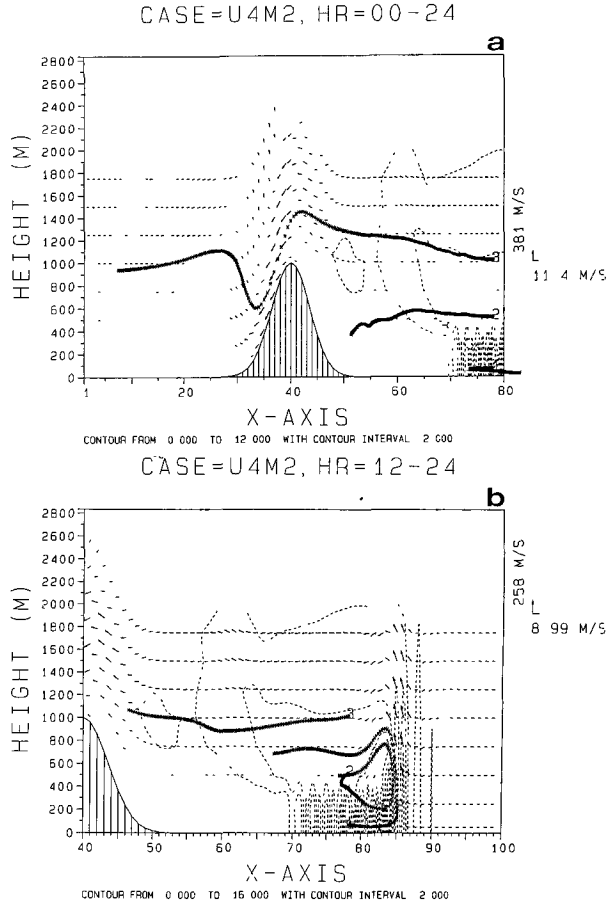

Fig. 13. The Lagrangian pathways of three particles released (a) initially and (b) at 12 h. The three particles were located at different heights of 50 m (Particle 1), 500 m (Particle 2) and 1 km (Partical 3). The interval of every two adjacent symbols in the pathways corresponds to a three-minute movement of the particle.

mountain waves as shown before. This indicates a nearly adiabatic isentropic trajectory for the flow at upper levels. Hence, the pollutant pathway can be estimated in the isentropic surface although the moist equivalent vorticity is not strictly conserved for moist flow as discussed in Bennetts and Hoskins (1979). In this figure, the concentration of the pollutants at 24 h is also plotted and is represented by dashed lines. As can be seen, the pollutant concentration at this time had been diffused upward to a level of 2 km and was well mixed at lower levels. As mentioned previously, the well-mixed pollution at low levels was due to the dominating turbulent processes.

Since the pathways of the particles assume initial release, later release at the same position may lead to significantly different results if the evolving flow does not reach a steady state. This is evidenced by the results of the three particles released at 12 h which exhibit quite different pathways. Indeed, Particles 1 and 2 released at this time did not move inland since the coastal flow deformation was prominent at this time. Particle 1 (at 50 m height) was forced to first move offshore and was then carried upward by the frontal updraft. As it reached higher levels, it underwent turning at upper levels. This turning was in response to the combined effects of the outflow divergence of the updraft and the onshore ambient force at upper levels. Partical 2 (at 500 m height), however, first sank into the low-level offshore flow and then experienced a movement similar to that of Particle 1. Particle 3 (at 1 km height) which sank slightly appeared to be weakly influenced by the coastal circulation and the mountain flow. From the results of Lagrangian particle pathways, we can infer that coastal air quality will become much worse as the coastal frontogenesis is strengthened to confine the pollutants near the coastal region. The release time and height of a particle are, thus, important for precise determination of its pathway during coastal frontogenesis.

V. Conclusions

Advection-diffusion processes of instantaneous pollutant source have been investigated for environmental conditions with coastal frontogenesis using a mesoscale planetary boundary layer numerical model. Model results show that the cloud and pollutant distributions were sensitive to ambient wind speed, moisture profile, wind shear and the height and location of mountain barrier. The effects of these factors have been discussed in detail in this study.

Within the marine boundary layer (MBL), redistribution of the coastal pollutants was predominantly determined by turbulent diffusion processes. Above the boundary layer, the movements of the pollutants essentially followed the cloud dynamics if the diffused pollutants had been transported into the clouds by the frontal updrafts. The near-surface pollutants over the ground, however, were not well-mixed vertically as a thin stable layer formed just behind the coastal front. A near-surface accelerating offshore flow formed over land during coastal frontogenesis in response to the induced pressure change over the coastal baroclinic zone. This offshore jet tended to impel the pollutants back into the coastal source region.

At the stage when the front remained shallow, the pollutants primarily followed the near-surface mean flow and were redistributed within the shallow stable layer. As the front intensified and developed to higher levels, the pollutants could be transported by the frontal updraft or diffused by the turbulence into the cloudy zone. The pollutants would be gradually diluted due to the wider spreading of the concentration volume. When the shear of the offshore flow was present, the coastal frontal updraft tended to move offshore with time. The offshore moving speed of the frontal updraft was found to be close to the ambient wind speed at the developed height of the MBL.

The mountain influences on the transportation of the coastal pollutants were investigated in this study. It was found that the height of the mountain barrier and the released height of the pollutants were two of the key factors for pollutant pathways. The coastal pollutants contaminated the far downstream region with much diluted concentration due to the expansion of its volume as expected. However, a large amount of the pollutants could be trapped near the coast if a big terrain barrier existed and was closer to the coastal region. This modeling study gives additional information concering pollution features over coastal complex terrain where observational data for the meso-γ (2-20 km) and meso-β scale (20-200 km) may be inadequate to describe the coastal pollution.

Acknowledgments

This research was supported by grant NSC 83-0202-M-008-030 from the National Science Council of the R.O. C. Computational support in the form of a VAX 9320 computer provided by the Computer Center of National Central University was greatly appreciated.

References

Anthes, R. A. and T. T. Warner (1978) Development of hydrodynamic models suitable for air pollution and other mesometeorological studies. *Mon Wea. Rev.*, **106**, 1045-1078.

Arritt, R. W., R. A. Pielke, and M Segal (1988) Variations of sulfur dioxide deposition velocity resulting from terrain-forced mesoscale circulations. *Atmos. Environ.*, **22**, 715-723.

Bennetts, D. A. and B. J. Hoskins (1979) Conditional symmetric instability-a possible explanation for frontal rainbands. *Quart. J. Roy. Meteor. Soc.*, **105**, 945-962.

Bornstein, R. D. and E. Runca (1977) Preliminary investigation of SO_2 patterns in Venice, Italy, using linked PBL and K models, including removal processes. *Preprints, Second Joint Conference on Applications of Air Pollution Meteorology (Salt Lake City)*, AMS, Boston, pp. 277-282

Bosart, L. F. (1975) New England coastal frontogenesis. *Quart. J. Roy. Meteor Soc.*, **98**, 735-744.

Emanuel, K. A. (1983) The Lagrangian parcel dynamics of moist symmetric instability. *J. Atmos. Sci.*, **40**, 2368-2376.

Hanna, S. R. (1982) Review of atmospheric diffusion models for regulatory applications WMO Tech. Note No. 177, WMO, Geneva, 33 pp.

Helfand, H. M. and J. C. Labraga (1988) Design of a nonsingular level 2.5 second order closure method for the prediction of atmospheric turbulence. *J. Atmos. Sci.*, **45**, 113-132.

Huang, C. Y. and S. Raman (1988) A numerical modeling study of the marine boundary layer over the Gulf Stream during cold air advection. *Bound. -Layer Meteor.*, **45**, 251-290.

Huang, C. Y. and S. Raman (1989) An application of the E- ε closure model to simulations of mesoscale topographic effects. *Bound.-Layer Meteor.*, **49**, 169-195.

Huang, C. Y. and S. Raman (1991a) Numerical simulation of January 28 cold air outbreak during GALE. Part I: The model and sensitivity tests of turbulence closures. *Bound.-Layer Meteor.*, **55**, 381-407.

Huang, C. Y. and S. Raman (1991b) Numerical simulation of January 28 cold air outbreak during GALE. Part II: The mesoscale circulation and marine boundary layer. *Bound.-Layer Meteor.*, **56**,51-81.

Huang, C. Y. and S. Raman (1991c) A comparative study of numerical advection schemes featuring a one-step modified WKL algorithm. *Mon. Wea. Rev.*, **119**, 2900-2918.

Huang, C. Y. and S. Raman (1992) A three-dimensional numerical investigation of a Carolina coastal front and the Gulf Stream rainband. *J. Atmos. Sci.*, **49**, 560-584.

Huang, C. Y. (1993) A study of high-order advection schemes in variable resolution. *TAO*, **4**, 421-440.

Huang, C. Y., (1994) Semi-Lagrangian advection schemes and Eulerian WKL algorithms. *Mon, Wea. Rev.*, **122**, 1647-1658.

Kessler, E. (1969) On the distribution and continuity of water substance in atmospheric circulation. *Meteorological Monographs*, **32**, 1-84.

Knight, D. and P. V. Hobbs (1988) The mesoscale and microscale structure and organization of clouds and precipitation in mid-latitude cyclones. Part XV: A numerical modeling study of frontogenesis and cold-frontal rainbands. *J. Atmos. Sci.*, **45**, 915-928.

MacCracken, M C., D. J. Wuebbles, J. J. Walton, W. H. Duewer, and K. Grant (1987) The Livermore regional air quality model: 1. concept and development. *J. Appl. Meteor.*, **17**, 254-272.

Mellor, G. L. and T. Yamada (1982) Development of a turbulence closure model for geophysical fluid problems. *Rev. Geophys. Space Phys.*, **20**, 851-875.

Pasquill, F. (1974) *Atmospheric Diffusion*, 2nd ed., John Wiley and Sons, New York.

Pielke, R. A., R. T. McNider, M. Segal, and Y. Mahrer (1983) The use of a mesoscale numerical model for evalutations of pollutant transport and diffusion in coastal regions and over irregular terrain. *Bull. Amer. Meteor. Soc.*, **64**, 243-249.

Pierrehumbert, R. T. and B. Wyman (1985) Upstream effects of mesoscale mountains. *J. Atmos. Sci.*, **42**, 977-1003.

Segal, M., R. T. McNider, R. A. Pielke, and D. S. McDougal (1982) A numerical model study of the regional air pollution meteorology of the Greater Chesapeake Bay area. *Atmos. Environ.*, **16**, 1381-1397.

Shir, C. C. and L. J. Shieh (1974) A generalized urban air pollution model and its application to the study of SO_2 distributions in the St. Louis metropolitan area. *J. Appl. Meteor* , **13**, 185-204.

Smith, R. B. (1979) The influence of mountains on the atmosphere. *Adv. Geophys.*, **21**, 87-230.

A Numerical Study of Pollutant Distributions

鋒面變形期間沿海空氣污染之數值研究

黃清勇

中央大學大氣科學系

摘　要

本文探討瞬間污染源於沿岸鋒生情況下平流與擴散的過程。研究方式爲使用一中尺度邊界層數值模式，此模式包含亂流閉合及雲微物理。系統性模擬實驗結果顯示，於鋒面變形期間，雲及污染物之分佈對環境風速、垂直濕度剖面與風切，以及附近地形障礙之高度與位置之變化皆相當敏感。本文詳細探討這些因子的作用，發現於此沿岸風場及穩定度多變情況下，污染物的平流與擴散過程相當複雜。本文亦探討亂流擴散與平均氣流傳送之相對重要性，特別針對污染源之高度與釋放時間。